

# How big is a small earthquake? Challenges in determining microseismic magnitudes

J-Michael Kendall<sup>1\*</sup>, Antony Butcher<sup>1</sup>, Anna L. Stork<sup>1</sup>, James P. Verdon<sup>1</sup>, Richard Lockett<sup>2</sup> and Brian J. Baptie<sup>2</sup> discuss the challenges in quantifying the size of small earthquakes induced in reservoir projects and provide a suggested monitoring strategy.

## Introduction

Earthquake magnitudes are surprisingly difficult to estimate accurately. This is especially true when evaluating small earthquakes: for example, those caused by human activities such as shale gas stimulation, CO<sub>2</sub> and waste water storage, and enhanced geothermal systems. Uncertainties are created by a range of issues including: which ‘magnitude’ scale is used; what type of instrument records the earthquake; how the instruments are deployed; and the heterogeneity of the Earth between the source and the receivers. Errors can be larger than an order of magnitude in scale. For very small earthquakes this is not usually of much concern. However, occasionally, larger earthquakes induced by human activity are felt at the surface. This has led to regulatory frameworks that require accurate assessment of earthquake magnitudes before they reach the point of being felt. Hence, to monitor and mitigate felt seismicity there is a need to calculate accurate earthquake magnitudes in real time. Regulatory monitoring of induced seismicity is becoming a key issue in the successful development of reservoir projects that involve stimulation or storage. Here, we discuss the challenges with implementing such reservoir monitoring, and provide a suggested monitoring strategy.

## Traffic light systems (TLS)

‘Traffic light systems’ (TLS) (e.g., Bommer et al., 2006) are sometimes used to mitigate induced seismicity, whereby operations are paused, stopped or amended based on the characteristics of the recorded seismicity. The purpose of a TLS is not to eliminate induced seismicity — all hydraulic fracturing is accompanied by very small magnitude seismic events (termed ‘microseismicity’) as the rock is fractured by the fluid pressure. The purpose of a mitigation scheme is usually to minimize the discomfort felt by the local public, and to eliminate the potential for damage to nearby buildings. In 2011, hydraulic fracture stimulation in the Preese Hall region of NE England led to a series of seismic events, the largest of which were felt at the surface (Clarke et al., 2014). This led to a moratorium on shale gas development in the UK and the implementation of a TLS for the UK. Figure 1 shows a comparison of TLS in operation in different parts of North America and the UK. The striking feature is the variability of the thresholds, reflecting public concern and variations in population density.

The UK has the strictest scheme of those highlighted in Figure 1: the TLS amber- and red-light limits are currently set at magnitudes of  $M = 0.0$  and  $M = 0.5$ , respectively. If the amber light is exceeded during pumping, the operator can continue pumping, but must perform a well integrity check. If the red light is exceeded during pumping the operator must immediately suspend injection, reduce pressure and monitor seismicity for any further events. The focal location and mechanism should be determined to see whether the seismicity is natural or, if induced, whether it accords with the assumptions and expectations set out in a hydraulic fracture plan, which in the UK must be submitted by the operator in advance of any injection. If the magnitude and ground motion of an induced seismic event conform with the assumptions and predictions in the hydraulic fracture plan, injection operations can resume after an 18-hour pause, subject to any mitigation or other measures as part of the agreed plan.

## Rock failure and earthquakes — a brief review

Earthquakes are caused by a sudden release of stress when forces are enough to break the rock or overcome the friction along a pre-existing plane of weakness (a fault or fracture). The magnitude of this seismic event describes the energy it releases. Every

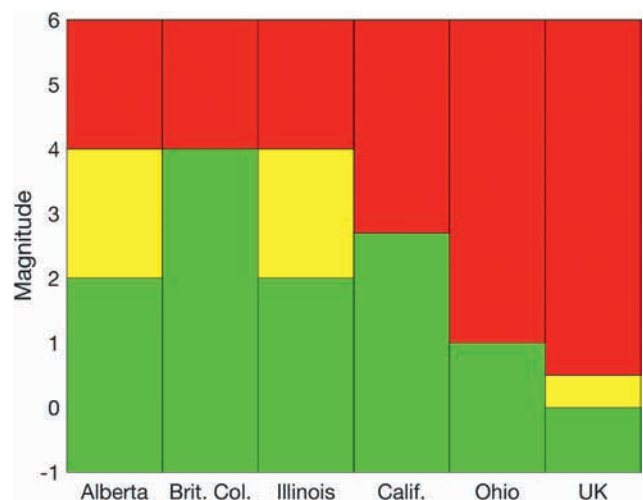


**Figure 1** ‘Traffic light system’ thresholds as applied by regulatory jurisdictions in Canada, US and the UK. The UK TLS has the lowest thresholds of any scheme used to regulate seismicity induced by hydraulic fracturing.

<sup>1</sup> University of Bristol, School of Earth Sciences | <sup>2</sup> British Geological Survey, Earthquake Seismology

\* Corresponding author, E-mail: gljmk@bristol.ac.uk

year millions of small earthquakes occur naturally and go largely undetected. This includes those generated by human activity. Monitoring small earthquakes or microseismicity is now a routine tool for evaluating hydraulic fracture stimulation in tight-gas sandstones, shale gas formations and geothermal reservoirs. Most stimulated events are very small, but occasionally larger felt events are induced through stimulation and fault reactivation. For this reason, regulatory monitoring is a growing concern and is required for longer time periods and over larger areas.

Rock failure occurs when shear-stresses ( $\sigma_s$ ) exceed the critical values described by the Mohr-Coulomb envelope,

$$\sigma_s = \tan \phi \sigma_n + C, \tag{1}$$

where ( $\sigma_n$ ) is the normal stress,  $C$  is the cohesion, and  $\phi$  is the internal friction. The latter two are intrinsic properties of the rock – stiffer rocks generally have higher coefficients of cohesion and steeper friction angles. Injection of fluids into the rock increase the pore pressure ( $P$ ) and reduce the effective normal stress ( $\sigma_n - P$ ). This means that earthquakes will occur at lower shear stresses. In the case of fault reactivation, a pre-existing weakness will have a lower cohesion or internal friction than the intact rock, again leading to rock failure at lower shear stresses. Faults may also be conduits for fluids, again reducing normal stresses.

Gutenberg and Richter (1944) showed that the magnitude–frequency relationship for an earthquake population follows a power-law behaviour,

$$\log_{10} N = a - bM, \tag{2}$$

where  $N$  is the number of events with a magnitude larger than  $M$ . This is the equation of a straight line where the intercept  $a$ -value describes the overall activity level within a region, and is the number of events with  $M \geq 0$ . The  $b$ -value is the slope of the line. A  $b$ -value of 1 implies that if there is 1 magnitude >3 event, there will be 10 magnitude >2 events, 100 magnitude >1 events, and so on. In global tectonic earthquake populations,  $b$  values are commonly observed to be close to 1. However,  $b$ -values can vary depending on the stress regime and the role of fluids. Often during hydraulic fracture stimulation, where fluids reduce the shear strength required to rupture the rock,  $b$ -values are much higher than unity (>2 is not uncommon).

In the context of hydraulic fracture stimulation, high  $b$ -values are good, indicating fluid-triggered development of a fracture network, and low stress build-up —  $b$ -values near unity indicate higher stress build-up and possible fault reactivation. Accurate  $b$ -values require accurate measurements of magnitude across a range of scales.

### The moment magnitude

There are a number of approaches to quantifying the size of a seismic event and thus far we have simply labelled the magnitude  $M$ . The moment magnitude ( $M_w$ ) is the preferred scale as it is directly related to fault dimensions, the amount of slip of the fault and energy release. The seismic moment,  $M_o$ , is defined as,

$$M_o = \mu s D, \tag{3}$$

where  $\mu$  is the shear modulus,  $s$  is the slip on the fault and  $D$  is the area of the fault that slips (see, e.g., Aki and Richards, 2002). The moment magnitude is defined as (Hanks and Kanamori, 1979),

$$M_w = 2/3 \log M_o - 6.07, \tag{4}$$

where  $M_o$  is measured in Nm. As these scales are logarithmic, each unit of magnitude increase relates to a ten-fold increase in displacement amplitude, which in turn corresponds to energy increasing by a factor of 32.

As we cannot directly measure the geometry of the fault and how it moves, we need to estimate the seismic moment through other methods. One approach is the use of the moment tensor, which is a mathematical representation of the magnitude and orientation of movement on a fault. However, this is time consuming to calculate and requires good station coverage. A more common approach for small magnitude seismic events is to evaluate the seismic moment from the moment function in the time or frequency domain (Figure 2) (e.g., Stork et al., 2014). This signal is a product of the convolution of the fault rupture time and the rise time and its integral is proportional to the moment (a force times distance) of the earthquake rupture. The seismic moment,  $M_o$ , in the frequency domain can be determined from the displacement pulse of a  $P$ - or  $S$ -wave arrival, and can be expressed as,

$$M_o = 4\pi\rho v^3 r \Omega_o / R, \tag{5}$$

where  $\rho$  is the density,  $v$  is the seismic velocity at the source (of the  $P$ - or  $S$ -wave, as appropriate),  $r$  is the source-receiver distance, and  $R$  is a radiation pattern correction. The term  $\Omega_o$  is the low-frequency level of the amplitude spectrum and is equal to the area under the displacement pulse (Figure 2).

$\Omega_o$  can be estimated from amplitude spectra that are corrected for attenuation effects. At high frequencies the amplitude

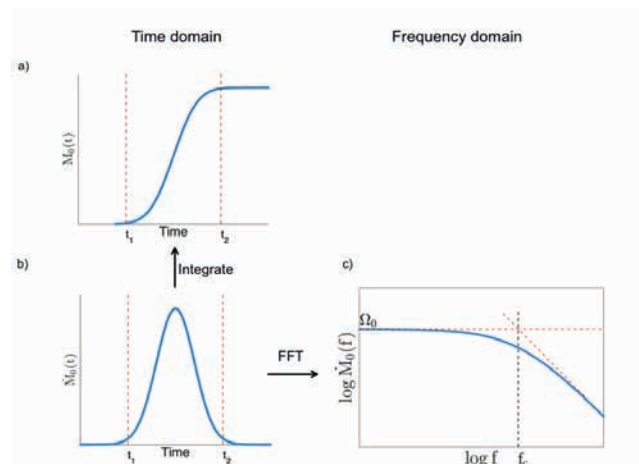


**Figure 2** Earthquake model in the time and frequency domain. (a) The moment time function,  $M_o(t)$ , is the change in moment due to earthquake slip along a fault. This increases over the duration of the event, between times  $t_1$  and  $t_2$ . (b) The seismic moment rate function,  $M_o'(t)$ , is proportional to the far-field displacement pulse (Aki and Richards 2002). (c) In the frequency domain, the moment rate spectrum is the Fourier transform of  $M_o'(t)$ . At low frequencies the spectral amplitude becomes constant ( $\Omega_o$ ) and is proportional to the seismic moment.  $f_c$  is the corner frequency and FFT is the fast Fourier transform.

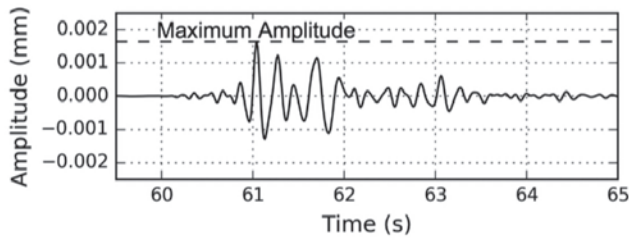


**Figure 3** Example of a seismic event where the maximum amplitude of the S-wave used to determine  $M_L$ .

of the signal decays linearly and the point at which this decay starts is known as the corner frequency,  $f_c$ . As attenuation,  $Q$ , is generally unknown, determining  $\Omega_0$  normally involves fitting for  $\Omega_0$ ,  $f_c$  and  $Q$  simultaneously using a Brune source model (see Stork et al. (2014) for details). Furthermore, when dealing with small events (*i.e.*, microseismic events, where  $f > 10$  Hz), the near-surface attenuates high-frequency energy making it difficult to estimate  $f_c$  (Anderson and Hough, 1984). The parameter,  $\kappa_0$ , accounts for high-frequency energy decay beyond a site-dependent maximum frequency,  $f_{max}$ . The so-called kappa-corrected Brune model is,

$$\Omega(f) = \frac{\Omega_0 e^{-(\pi f r / v Q)}}{[1 + (f / f_c)^2]} e^{(-\pi f \kappa_0)}, \quad (6)$$

which is based on the traditional Brune source model with an additional exponential term involving  $\kappa_0$  (Batlay and Hanks, 2014). This term is site dependent and there are range of approaches to estimate  $\kappa_0$  (see, *e.g.*, Ktenidou et al., 2014).

A number of factors can lead to significant errors in the estimation of  $M_w$  and, without care, variations of a unit in magnitude can be produced (Stork et al., 2014). The most significant errors can be caused by a failure to calculate the radiation pattern for the earthquake correctly (often a time-consuming exercise). This requires good station coverage and it is recommended that at least four stations with good azimuthal coverage are used. The calculations should be made for both the *P*- and *S*-wave phases. A correction for free-surface effects should also be included for stations deployed on the surface. Sampling rates need to be high enough to capture the corner frequency,  $f_c$ , which for  $M_w \leq 0$  requires sampling rates  $> 1000$  Hz. Another issue concerns the nature of the seismic sensor. A broadband instrument is required to capture the low-frequency signal needed to accurately record  $\Omega_0$  (Baig et al., 2010). In addition, a *Q*-corrected amplitude spectra should also be used and a correction for  $\kappa_0$  should be applied if possible. Finally, good knowledge of the seismic velocity at the source is important, as it is cubed in equation (5), and it also affects the accuracy of the event location.

Estimating the moment magnitude,  $M_w$ , is easy in principle, but can be time consuming and requires a good signal-to-noise ratio. As most hydraulic stimulation stages generate thousands of earthquakes, we need a quicker method to estimate the source magnitude. The easiest approach is to use the largest observed amplitude of displacement recorded on a seismometer. This is the basis of the local magnitude, which follows the form of the original magnitude scale proposed by Richter (1935).

## The local magnitude

The idea of local magnitude ( $M_L$ ) was developed by Charles Richter in 1935, and is an empirical scale based on the ground displacement recorded on a particular type of instrument in southern California (Richter, 1935).  $M_L$  was a scale based on a  $M=3$  representing 1 mm of displacement on the horizontal-component of a Wood–Anderson seismometer at a distance of 100 km from the epicentre. The general form of a local magnitude scale is,

$$M_L = \log(A) - \log(A_0), \\ = \log(A) - (a \log(r) + b(r) + c), \quad (7)$$

where  $r$  is the hypocentral distance. The term ( $\log(A_0)$ ) is a displacement correction term, which is comprised of three terms to be applied for geometrical spreading, attenuation and a base level, respectively.  $A$  is the zero-to-peak displacement amplitude measured by a seismometer (Figure 3), where its response has been converted to that of a short-period Wood-Anderson seismometer, an instrument that is no longer in routine use. This correction is broadly comparable to a 2 Hz high-pass filter and a gain correction of 2080.

The analysis of amplitudes from earthquakes in a given region (*e.g.*, the UK) recorded by stations at a range of epicentral distances can be inverted to determine local values for the terms in the equation (7). For example, based on nearly 1500 observations from 85 earthquakes recorded by 50 stations, Ottemöller and Sargeant (2013) determined the following local magnitude scale for the UK,

$$M_L = \log(A) + 0.95 \log(r) + 0.00183(r) - 1.76. \quad (8)$$

The nominal detection level for the UK network is  $M_L = 2.0$  and most stations are more than 50 km from any given earthquake. Furthermore, most earthquakes are tectonic in nature and lie in the middle crust ( $>10$  km in depth), so the recorded seismic waves have travelled primarily through deeper, crystalline crustal rocks (Figure 4).

In most industrial applications of earthquake monitoring (*e.g.*, shale gas stimulation), seismometers are deployed very close to the site ( $<10$  km) and the earthquakes are shallow ( $<4$  km) (Figure 4). As a result, seismic waves travel primarily through the low-velocity and highly-attenuating near-surface. This leads to a systematic overestimation of seismic local

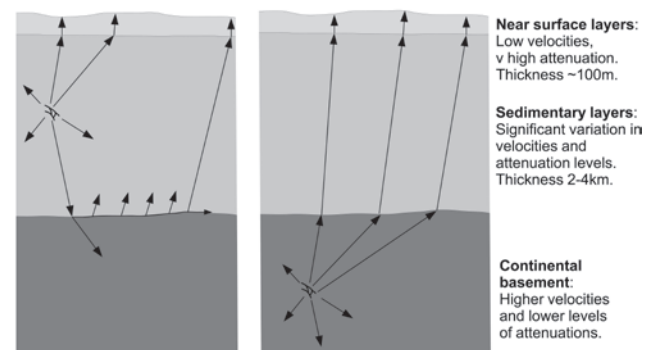


**Figure 4** Schematic travel paths for: (left) shallow earthquake occurring in sedimentary layers; (right) deeper regional tectonic event.

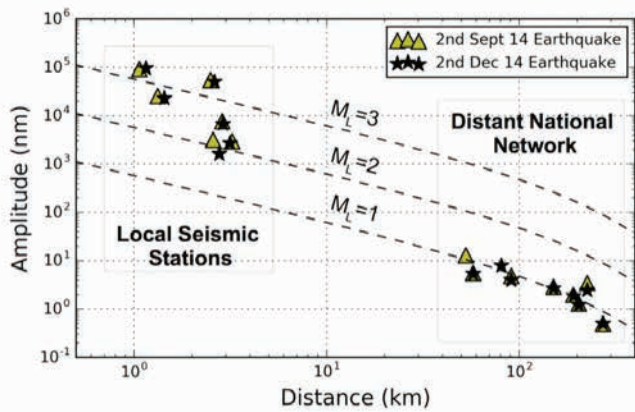


**Figure 5** Recorded displacement amplitude versus distance for two coal-mining related earthquakes, as shown by stars and triangles, recorded by 14 stations. The dashed lines show the corresponding magnitudes based on the UK scale for  $M_L$  1.0, 2.0, and 3.0 (i.e., using equation (8)). Amplitudes recorded on stations <5 km from the epicentre systematically estimate much larger magnitudes than those recorded by stations >50 km from the epicentre. See Butcher et al. (2017) for more detail.

magnitudes, as the largest waveform now relates to a different phase than that used to originally derive the scale (Butcher et al., 2017). Figure 5 shows the recorded displacement amplitudes for two coal-mining-induced events in NE England (described by Verdon et al., 2017) recorded by six stations in a local seismic array (<5 km) and eight stations from the regional UK array that are >50 km from the events. On the distant stations, the displacements match well with the UK scale for an  $M_L$  1.0 event. On the nearby stations, displacements are substantially larger, and this discrepancy increases as the hypocentral distance decreases.

To address this limitation a modified local magnitude scale is required for stations less than a critical distance. In this case that distance was selected at 17 km, but this is dependent on the local geology and will vary from region to region. Based on the analysis of a cluster of similar coal-mining-induced seismic events, Butcher et al. (2017) have developed a modified UK local magnitude scale for events in northern England where the source-receiver distance is less than 17 km,

$$M_L = \log(A) + 1.17 \log(r) + 0.0514(r) - 3.0. \quad (9)$$

Hence two  $M_L$  scales should be used – the UK scale (8) when the source-receiver separation is greater than 17 km, and the Butcher scale (9) when stations are < 17 km from the source. The biggest difference between equations (9) and (8) is in the attenuation terms, which are over an order of magnitude different in size (0.0514 versus 0.00183). More recently, Luckett et al. (2019) have combined the two scales using an exponential term to measure the near and far offset contributions, as adopting an entirely new scale would require the BGS to recalculate and republish its entire catalogue. This scale is expressed by

$$M_L = \log(A) + 1.11 \log(r) + 0.00189(r) - 2.09 - 1.16e^{-0.2r}, \quad (10)$$

which is the same as the scale used to estimate  $M_L$  in the UK, but corrects for the overestimation of magnitudes at near offsets. Recently this has been adopted for all UK  $M_L$  calculations.

### Finding the right moment: $M_w$ versus $M_L$

The moment magnitude scale was developed to address the well-known deficiency that local magnitude scales break down at large magnitudes. For example, the devastating 2011 Tohoku earthquake had a moment magnitude of  $M_w$  9.1, but early estimates of the local magnitude were  $\sim M_L$  7.9. This is explained by saturation issues, where both the amplitudes and the frequency range are beyond the sensitivity of the instrument. Large earthquakes typically generate the majority of their energy at low frequencies (i.e. <1 Hz), which is removed when estimating  $M_L$ , mainly due to the correction to a shorter-period Wood-Anderson response (Figure 6).

As previously discussed,  $M_L$  scales break down at small magnitudes, as microseismic events rarely contribute to the derivation of these empirical scales. This is partially because there was little historical interest in capturing these types of earthquakes, as a result of difficulties in recording them. In his 1958 textbook, Richter states that ‘comparatively little can be accomplished with seismograms belonging to the local earthquake range of distance’, as instrument timing of this period could not accurately record these higher-frequency events. Although this has been overcome in modern-day instruments, they are still challenging to record, as to achieve good signal-to-noise ratios requires receivers located at distances typically <10 km from the source. As a result, complete microseismic catalogues are rare and often only cover a very localized region.

Even when they are well recorded, local magnitudes are regularly observed to be smaller than moment magnitudes for magnitudes less than 3, with this discrepancy increasing as the size of the event decreases. The primary cause of this discrepancy is due to a preferential decay of high-frequency energy as it propagates through highly attenuating layers (Deichmann, 2017), such as the near-surface (Figure 4). These act to reduce the maximum amplitude in the time-domain. Magnitudes calculated using  $M_L$  will therefore be smaller than  $M_w$ .  $M_w$  is estimated using the low-frequency plateau,  $\Omega_0$ , in equation (5), and is therefore unaffected by the loss of high frequencies (Figure 6).

Furthermore,  $M_w$  is often preferred by seismologists, as it is directly related to the seismic moment ( $M_0$ ), which is the best measure of earthquake size. Nevertheless, it can be difficult to estimate accurate moment magnitudes with the low signal-to-noise ratios characteristic of these small events. It is therefore desirable to correct local magnitudes to infer moment magnitudes and the seismic moment. A comparison of local and moment magnitudes can be used to establish a  $M_L$  correction for a given region (e.g., Munafò et al., 2016). Having this correction allows a prediction of  $M_0$  from  $M_L$ .

As shown in equation (3),  $M_0$  is related to the amount of slip on a fault plane. However, there is an ambiguity in that large slip on a small fault plane is equivalent to small slip on a large plane. This is important, as the stress drop is different in each scenario. To better establish the fault area (and hence slip) and stress drop requires not only knowledge of the seismic moment ( $M_0$ ), but also the corner frequency ( $f_c$ ). As noted, attenuation in near-surface layers imposes a maximum frequency limit,  $f_{max}$ , leading to errors in estimates of  $f_c$  (see Figure 6), and hence errors in estimates of

fault dimension and stress drop. These errors are most significant at the seismic station close to an earthquake, and can produce differences in stress drops of up to two orders of magnitude. As mentioned, an estimate of  $\kappa_o$  is a useful approach to obtain accurate corner frequencies,  $f_c$ , and numerous different approaches for estimated  $\kappa_o$  are reviewed by Ktenidou et al. (2014). One such approach that is being currently explored is to use the ambient noise field to estimate the decay of high frequencies, which can be measured prior to operations that may result in microseismicity. This can allow for the development of physics-based relationships between  $M_L$  and  $M_w$ , and more accurate estimation of the properties of an earthquake.

## Conclusions

The increasing use of traffic light systems (TLS) to regulate induced seismicity in a range of settings requires accurate estimates of earthquake magnitudes in real time. However, there are a number of factors that lead to errors in estimates of seismic magnitudes. The use of the moment magnitude ( $M_w$ ) is preferable as this scale leads to an assessment of fault dimensions and stress release. However, in practice local magnitudes ( $M_L$ ) are simpler to use, especially in real-time applications. Measurements of microseismicity using either scale are affected by the local geology and near-surface attenuation. Getting things right involves using appropriate instruments, well placed sensor arrays and a good understanding of the near surface.

Accurate determination of the seismic moment ( $M_o$ ) based on spectral estimates requires instruments with a broadband response, a high (>1000 Hz) sample rate and a good signal-to-noise ratio. The spectra should be rich in low-frequency signal and a correction for  $Q$ , and  $\kappa_o$  if possible, is important. Estimates should be made from both  $P$ - and  $S$ -wave phases, using four or more stations deployed with good azimuthal coverage of source radiation patterns. A good knowledge of uncertainties in the velocity model and event locations should also be taken into account.

The use of local magnitude scales ( $M_L$ ) requires careful calibration, as the scales will vary in form from region to region. Furthermore, signals recorded near the source will

have a tendency to overestimate magnitudes in comparison with signals recorded at stations with epicentral distances of more than 15-20 km. This is because raypaths to the near-offset stations travel through more highly attenuating near-surface sedimentary layers. Raypaths to more distant stations are primarily through less-attenuative basement rocks. A separate magnitude scale must be therefore derived for the near-offset stations, which requires knowledge of baseline natural- and/or induced-seismicity in a region.

Moment and local magnitudes diverge with large earthquakes (> M 6.0), but also with microseismic earthquakes (< M 2.0). The former is due to saturation issues, as  $M_L$  is calculated using a Wood-Anderson instrument response, with frequencies lost below ~2 Hz.  $M_w$  should always be used for large events. The latter relates to a preferential attenuation affecting high frequencies (>10 Hz). A regional comparison of  $M_L$  and  $M_w$  can be used to develop a correction. Furthermore, a correction for the exponential loss of high-frequency energy is required to ensure accurate estimates of earthquake parameters such as fault dimensions, fault slip and stress drop.

In conclusion, monitoring arrays that address operator needs (e.g., low detection thresholds) will be very different from arrays required for regulatory purposes (e.g., accurate magnitudes). As induced seismicity continues to attract public attention, the next few years will likely see the rapid development of monitoring strategies for regulatory purposes.

## Acknowledgements

This work has been funded by the Bristol University Microseismic Projects (BUMPS), an industry-funded consortium (<https://www1.gly.bris.ac.uk/BUMPS>). Additional funding comes from the Natural Environment Research Council (NERC) Grant Numbers NE/R018006/1 'Impact of hydraulic fracturing in the overburden of shale resource plays: Process-based evaluation (SHAPE-UK)', NE/L008351/1 'Microseismic impact assessment for shale-gas stimulation (MIA)' and NE/L002779/1 'Microseismic monitoring for operators and regulators (MORE)'. JMK and AB are supported through funding from the British Geological Survey.

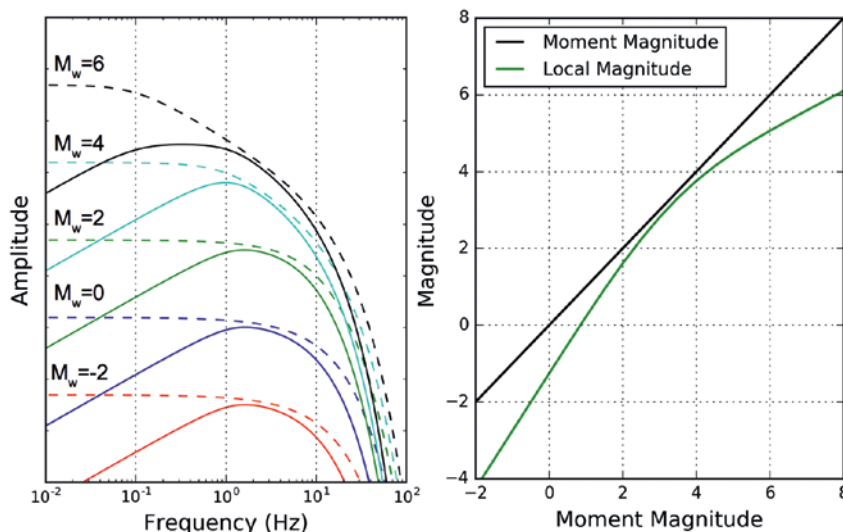


**Figure 6** (Left) Dashed lines show the modelled frequency content of earthquake sources varying in moment magnitude from -2 to 6. The solid lines show the frequency content after including a Wood-Anderson instrument response and including the effects of near-surface attenuation on the high frequencies. (Right) Schematic Figure showing differences between  $M_L$  and  $M_w$  as derived from the source spectra on the left. Note that  $M_L$  is derived from the spectra shown in solid lines, and  $M_w$  is from those in dashed lines.  $M_L$  underestimates magnitudes when they are large and small.

References

Aki, K. and P.G. Richards [2002]. *Quantitative Seismology, 2nd edition*, University Science Books, Sausalito.

Anderson, J.G. and S.E. Hough [1984]. A model for the shape of the fourier amplitude spectrum of acceleration at high frequencies. *Bulletin of the Seismological Society of America*, **74**(5), 1969-1993.

Baig, A. and T. Urbancic [2010]. Magnitude determination, event detectability, and assessing the effectiveness of microseismic monitoring programs in petroleum applications. *CSEG Recorder*, **35**(2), 22-26.

Baltay, A.S. and T.C. Hanks [2014]. Understanding the magnitude dependence of PGA and PGV in NGA-West 2 data. *Bulletin of the Seismological Society of America*, **104**(6), 2851-2865.

Bommer, J.J., S. Oates, J.M. Cepeda, C. Lindholm, J. Bird, R. Torres, G. Marroquin, J. Riva [2006]. Control of hazard due to seismicity induced by a hot fractured rock geothermal project. *Engineering Geology*, **83**, 287-306.

Butcher, A., R. Luckett, J.P. Verdon, J.-M. Kendall, B. Baptie, J. Wookey [2017]. Local magnitude discrepancies for near-event receivers: Implications for the UK Traffic Light Scheme. *Bulletin of the Seismological Society of America*, **107**, 532-541.

Clarke, H., L. Eisner, P. Styles, and P. Turner [2014]. Felt seismicity associated with shale gas hydraulic fracturing: The first documented example in Europe. *Geophysical Research Letters*, **41**(23), 8308-8314.

Deichmann, N. [2017]. Theoretical Basis for the Observed Break in  $M_L/M_w$  Scaling between Small and Large Earthquakes. *Bulletin of the Seismological Society of America*, **107**(2), 505-520.

Gutenberg, B., and C.F. Richter [1944]. Frequency of earthquakes in California. *Bulletin of the Seismological Society of America*, **34**, 185-188.

Hanks, T. C., and H. Kanamori [1979]. A moment magnitude scale. *Journal of Geophysical Research*, **84**(B5), 2348-2350.

Hutton, L. K., and D.M. Boore [1987]. The  $M_L$  Scale in Southern California. *Bulletin Of The Seismological Society Of America*, **77**(6), 2074-2094.

Ktenidou, O.J, F. Cotton, F.A. Abrahamson and J.G. Anderson [2014]. Taxonomy of  $K_L$ : a review of definitions and estimation approaches targeted to applications. *Seismological Research Letters*, **85**(1), 135-146.

Luckett, R., L. Ottemöller, A. Butcher and B. Baptie [2019]. Extending local magnitude  $M_L$  to short distances. *Geophysical Journal International*, **216**(2), 1145-1156.

Munafò, I., L. Malagnini and L. Chiaraluce [2016]. Short Note On the Relationship between  $M_w$  and  $M_L$  for Small Earthquakes. *Bulletin of the Seismological Society of America*, **106**(5), 2402-2408.

Ottemöller, L., and S. Sargeant [2013]. A local magnitude scale  $M_L$  for the United Kingdom. *Bulletin of the Seismological Society of America*, **103**(5), 2884-2893.

Richter, C.F. [1935]. An instrumental earthquake magnitude scale. *Bulletin of the Seismological Society of America*, **25**, 1-32.

Stork, A.L., J.P. Verdon and J-M. Kendall [2014]. The robustness of seismic moment and magnitudes estimated using spectral analysis. *Geophysical Prospecting*, **62**, 862-878.

Verdon, J.P., J-M. Kendall, A. Butcher, R. Luckett and B.J. Baptie [2018]. Seismicity induced by longwall coal mining at the Thoresby Colliery, Nottinghamshire, U.K. *Geophysical Journal International*, **212**(2), 942-954.

ADVERTISEMENT

HELD UNDER THE PATRONAGE OF HIS EXCELLENCY ABDEL FATTAH EL SISI PRESIDENT OF THE ARAB REPUBLIC OF EGYPT / تحت رعاية فخامة الرئيس عبد الفتاح السيسي رئيس جمهورية مصر العربية



**EGYPS**  
EGYPT PETROLEUM SHOW


11-13 February 2019  
Egypt International Exhibition Center


SUPPORTED BY



**NORTH AFRICA AND THE MEDITERRANEAN**  
DELIVERING THE ENERGY NEEDS OF TOMORROW

**REGISTER TO ATTEND THE LEADING OIL & GAS TECHNICAL CONFERENCE**

 <b>33</b> TECHNICAL SESSIONS	 <b>132</b> TECHNICAL SPEAKERS	 <b>32</b> TECHNICAL POSTERS	 <b>11</b> TECHNICAL CATEGORIES	 <b>3</b> DAYS
---	--	--	--	--

-  Oil, Gas and Unconventional Field Developments (OGUFD)
-  E&P Geoscience (GEO)
-  Gas Processing Technology and Operations (GPTO)
-  Drilling and Completions (DC)
-  Project Management, Engineering Technology and Implementation (PMETI)
-  Offshore Technology and Operations (OTO)

-  Downstream: Refining Technology, Operations and Marketing (DRTOM)
-  Operational Excellence, Maintenance and HSE (OEMH)
-  Gas to Power Generation Technology and Operations (PGTO)
-  Downstream: Petrochemicals Technology, Operations (DPTO)
-  Artificial Intelligence and Connected Performance Technology and Services (AKPTS)

4 EASY WAYS TO REGISTER


[www.egyps.com/confreg](http://www.egyps.com/confreg)

[egyps.delegate@dmgeventsme.com](mailto:egyps.delegate@dmgeventsme.com)

+971 2 697 0517, +2022 753 8402

+971 2 444 4383

SUPPORTED BY



DIAMOND SPONSORS




PLATINUM SPONSOR



GOLD SPONSORS



SILVER SPONSORS



BRONZE SPONSORS



OFFICIAL PUBLICATIONS



CO-ORGANISED BY

